On the fossil and non-fossil fuel sources of carbonaceous aerosol with radiocarbon and AMS-PMF methods during winter hazy days in a rural area of North China plain

Zhang, Yangmei; Zhang, Xiaoye; Zhong, Junting; Sun, Junying; Shen, Xiaojing; Zhang, Zhouxiang; Xu, Wanyun; Wang, Yaqiang; Liang, Linlin; Liu, Yusi; Hu, Xinyao; He, Ming; Pang, Yijun; Zhao, Huarong; Ren, Sanxue; Shi, Zongbo

DOI:
10.1016/j.envres.2021.112672

Document Version
Peer reviewed version

Citation for published version (Harvard):
Zhang, Y, Zhang, X, Zhong, J, Sun, J, Shen, X, Zhang, Z, Xu, W, Wang, Y, Liang, L, Liu, Y, Hu, X, He, M, Pang, Y, Zhao, H, Ren, S & Shi, Z 2022, 'On the fossil and non-fossil fuel sources of carbonaceous aerosol with radiocarbon and AMS-PMF methods during winter hazy days in a rural area of North China plain', *Environmental Research*, vol. 208, 112672. https://doi.org/10.1016/j.envres.2021.112672

On the Fossil and Non-fossil fuel Sources of Carbonaceous Aerosol with Radiocarbon and AMS-PMF Methods during Winter Hazy Days in a Rural Area of North China Plain

Yangmei Zhang,[a,*] Xiaoye Zhang,[a,b] Junting Zhong,[a] Junying Sun,[a] Xiaojing Shen,[a] Zhouxiang Zhang,[c] Wanyun Xu,[a] Yaqiang Wang,[a] Linlin Liang,[a] Yusi Liu,[a] Xinyao Hu,[a] Ming He,[d] Yijun Pang,[d] Huarong Zhao,[a] Sanxue Ren,[a] Zongbo Shi[e,*]

[a]State Key Laboratory of Severe Weather/Key Laboratory of Atmospheric Chemistry of China Meteorological Administration, Chinese Academy of Meteorological Sciences, Beijing 100081, China

[b]Center for Excellence in Regional Atmospheric Environment, IUE, Chinese Academy of Sciences, Xiamen 361021, China

[c]Hubei Ecological Environment Monitoring Center Station, Wuhan 430072, China

[d]Department of Nuclear Physics, China Institute of Atomic Energy, Beijing 102413, China

[e]School of Geography Earth and Environmental Sciences, The University of Birmingham, Birmingham B15 2TT, U.K.

Correspondence to: YM Zhang (ymzhang@cams.ac.uk) and ZB Shi (z.shi@bham.ac.uk)

Abstract

Regional transport is a key source of carbonaceous aerosol in many Chinese megacities including Beijing. The sources of carbonaceous aerosol in urban areas have been studied extensively but are poorly known in upwind rural areas. This work aims to quantify the contributions of fossil and non-fossil fuel emissions to carbonaceous aerosols at a rural site in North China Plain in winter 2016. We integrated online high resolution-time of flight-aerosol mass spectrometer (HR-TOF-AMS) observations and radiocarbon (^{14}C) measurements of fine particles with Positive Matrix Factorization (PMF) analysis as well as Extended Gelencsér (EG) method. We found that the fine particle concentration is much higher at the rural site than in Beijing during the campaign (7th Dec 2016 to 8th Jan 2017). PMF analysis of the AMS data showed that coal-combustion related organic aerosol (CCOA + Oxidized CCOA) and more oxidized oxygenated organic aerosol (MO-OOA) contributed 48% and 30% of organic matter to non-refractory PM_1 (NR-PM_1) mass. About 2/3 of the OC and EC were from fossil-fuel combustion. By EG method, combining AMS-PMF and ^{14}C data, we found that primary and secondary OC from fossil fuel contribute 35% and 22% to total carbon (TC), coal combustion emission dominates the fossil fuel sources, and biomass burning accounted for 21% of carbonaceous aerosol. In summary, our results confirm that fossil fuel combustion was the dominant source of carbonaceous aerosol during heavy pollution events in the rural areas. Significant emissions of solid fuel carbonaceous aerosols at rural areas can affect air quality in downwind cities such as Beijing and Tianjin, highlighting the benefits of energy transition from solid fuels to cleaner energy in rural areas.

Keywords： Air pollution; Fossil and non-fossil fuel emission; Coal combustion; Biomass burning; Sources apportionment;

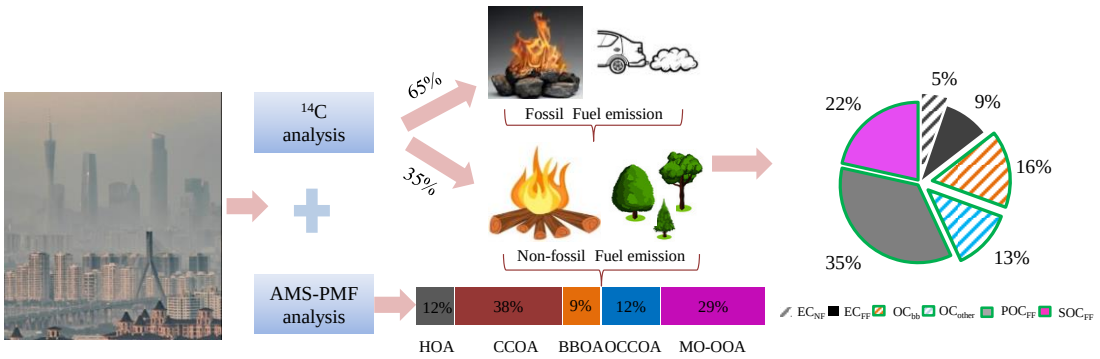

Graphical Abstract

1 Introduction

Atmospheric particles, especially with diameter less than 2.5 μm ($PM_{2.5}$) have a major influence on visibility (Watson, 2002) and human health (Pope III et al., 2002). They also exert direct (absorption and scattering) and indirect impacts (cloud interaction) on the climate through changing the Earth's energy balance (IPCC, 2021). Submicron particles (PM_1) contribute the most to these effects because their sizes are closer to the wavelength of visible light and they can penetrate deep into the respiration system (Costa et al., 2015; Marseglia et al., 2019; Pope and Dockery, 2006). It is estimated that $PM_{2.5}$ pollution has led to over 1 million premature deaths (GBD MAPS Working Group, (2016), and over 346 billion RMB in economic loss per year in China (Xia et al., 2016).

In China, frequent haze events have beset its air quality for decades. Since 2013, a series of clean air policies have substantially reduced mass concentration of particulate matter ($PM_{2.5}$) (Vu et al., 2019; Zhang et al., 2020). However, $PM_{2.5}$ levels are still several times higher than the newly announced air quality guidelines by the World Health Organization (WHO) (Cheng et al., 2021; WHO, 2021). Furthermore, serious haze events still occurred frequently, especially during wintertime in Northern China (Shi et al., 2021; Sun et al., 2015; Xu et al., 2021; Zhang et al., 2018; Zhang et al., 2017b). $PM_{2.5}$ pollution remains a major challenge in China.

Carbonaceous aerosol is a major component in PM_1, contributing 20-90% of PM_1 mass (Jimenez et al., 2009). Carbonaceous aerosol comprises a wide variety of organic compounds, generally referred as organic matter (OM), elemental carbon (EC), and carbonate, while the latter typically being negligible in submicron aerosol since it is mainly present in the coarse fraction (Sillanpää et al., 2005). OM is often referred as organic aerosol (OA), which is classified into primary and secondary organic aerosol (POA and SOA), the latter of which are formed from the condensation of oxygenated volatile organic compounds (OVOCs) or atmospheric oxidation of primary organic aerosol(Xu et al., 2021; Zhang et al., 2018). POA and its precursors can be emitted from fossil (e.g. coal combustion and vehicle exhaust) and non-fossil sources (e.g. biomass burning, vegetation emission, cooking) (Hou et al., 2021; Minguillón et al., 2011; Sun et al., 2019).

Although much progress has been made in the past 20 years in organic aerosol characterization and source apportionment (Hopke et al., 2020; Jimenez et al., 2009; Li et al., 2017b; Liang et al., 2016; Wang et al., 2021a; Zhou et al., 2020), it remains a major challenge to quantitatively determine the contributions of different sources to OA, not only for its complex origins but also for the unclear formation processes (Liang et al., 2016; Zhang et al., 2014b; Zhou et al., 2020). Chemical Mass

Balance (CMB) is an effective method to apportion the sources of organic carbon (OC) but it requires the analysis of a wide range of organic tracers and chemical profiles of PM from different sources in the local study region (Xu et al., 2020). Radioisotope of carbon (^{14}C) is an ideal tracer for distinguishing fossil and contemporary carbon. Due to its age (half life time 5730 years), ^{14}C is completely depleted in fossil-fuel emissions whereas non-fossil carbon sources (e.g. biomass burning or biogenic emissions) contain contemporary ^{14}C (Heal, 2014; Szidat, 2009). Filter-based radiocarbon analyses apportioned the sources of fossil and non-fossil to particulate matter in China (Hou et al., 2021; Liu et al., 2017; Liu et al., 2020; Zhang et al., 2017a; Zhou et al., 2017). Positive matrix factorization (PMF) (Ulbrich et al., 2009) and a multilinear engine (ME-2) (Canonaco et al., 2013) modelling of high time resolution organic mass spectrometric data from aerosol mass spectrometer (AMS) have also been used to resolve organics into various OA factors, which correspond to different sources and processes. OA are generally de-convolved into four POA (i.e. hydrocarbon OA (HOA), coal combustion OA (CCOA), food cooking OA (COA), biomass burning OA (BBOA)) and two SOA factors (i.e. less oxidized OA (LO-OOA) and more oxidized OA (MO-OOA)) (Sun et al., 2018; Zhang et al., 2018). HOA is generally considered from diesel/gasoline combustion. The exact sources of LO-OOA and MO-OOA remain unclear. Some studies argued that certain OOAs are oxidized HOA or CCOA based on their correlation markers such as nitrate and NO_2 or sulfate and SO_2 respectively (Sun et al., 2018; Zhang et al., 2018). However, the contributions from fossil and non-fossil fuel sources to carbonaceous aerosols remain poorly quantified.

North China Plain (NCP), including Beijing, Tianjin and Hebei, remains one of the most polluted city clusters in China. Although air quality in Beijing has improved significantly in the past few years as a result of the clean air actions (Li et al., 2021b; Vu et al., 2019; Zhang et al., 2020), Beijing still experiences frequent haze pollution events in the winter. Modelling and observations consistently suggest that a large fraction of the air pollutants in Beijing is from regional transport, and this is particularly true during hazy events (Cheng et al., 2018; Shi et al., 2021; Wang et al., 2021b; Zheng et al., 2015). Several observational studies in urban Beijing suggested that air pollutants transported from the south and southwest contribute significantly to air pollution in Beijing (Li et al., 2017a; Sun et al., 2018; Zhang et al., 2018; Zhong et al., 2020). Modelling studies also indicated that about half of the black carbon and carbon monoxide in Beijing is from regional transport (Liu et al., 2019; Panagi et al., 2020). Some studies on gaseous pollutants and PM composition were also carried out at upwind locations of Beijing, such as Gucheng (Kuang et al., 2020; Li et al., 2021a; Lin et al., 2009; Shi et al., 2021; Xu et al., 2021; Zhang, 2011; Zhong et al., 2020), Tianjing (Fan et al., 2020; Wang et al., 2020; Zhang, 2011; Zou et al., 2017) , Yufa (Takegawa et al., 2009) and Xianghe (He et al., 2021; Wang et al., 2021c; Wang et al., 2020). A major focus of these studies is to understand the formation mechanisms of secondary aerosol, particularly inorganic aerosols. However, little is known on the sources of carbonaceous aerosol in the upwind area of Beijing and Tianjin, particularly at rural areas (Xu et al., 2020).

In this study, we quantified the contribution of fossil fuel and non-fossil fuel combustion sources to carbonaceous aerosol at an upwind rural site of megacities, such as Beijing and Tianjin, in NCP. We chose a rural site at Gucheng, which is often downwind of industrial cities, namely Taiyuan, Shijiazhuang, Hengshui and upwind of Beijing and Tianjin (Kuang et al., 2020; Li et al., 2021a; Zhong et al., 2020). Gucheng is a typical regional background site in NCP. In the main manuscript, we firstly provide an overview of the PM_1 chemical composition and source

apportionment results during an intensive observation campaign from December 2016 to January 2017 (section 3.1). We then used the radiocarbon data to apportion the sources of fossil and non-fossil fuel combustion to OC and EC (Section 3.2). Finally, we combined the AMS-PMF results with ^{14}C-based extended Gelencsér (EG) method (Hou et al., 2021) to apportion the contribution of specific sources of carbonaceous aerosols (section 3.3) to OC.

2 Experiment section

2.1 Sampling site and instrumentation

All measurements were conducted at the Integrated Ecological-Meteorological Observation and Experiment Station of Chinese Academy of Meteorological Sciences, Gucheng station, in Hebei province (39°08′ N, 115° 40′ E, 15.2 m asl) (Figure 1). The area is representative of the wider rural areas in NCP, and has been chosen by previous studies to investigate regional sources and processes of air pollution in NCP (Lin et al., 2009;Li et al., 2021; Zhang, 2011). On a regional scale, the site locates within a pollution transport convergence belt of NCP. When the northwest winds from Mt. Yan and Taihang meet the southeast wind from the plain, the air masses form a transport convergence belt alongside the mountain. This is also called as an accumulation belt for the pollution of NCP (Su et al., 2004). On a local scale, it is surrounded by agricultural fields (for cultivation of wheat and corn), and the closest residential town (Dingxing county) is 15 km to the northeast of the site. There are no agricultural activities during the winter period. A national (arterial) road goes across the county which is 1.5 km away from the site.

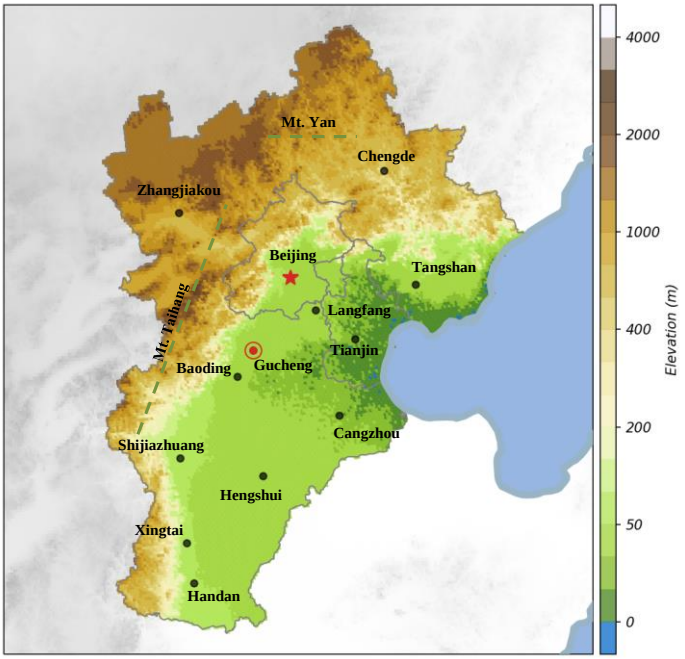

Figure1. The location of study site (red circle) and surrounding major cities in the NCP. The color scheme represents the elevation.

The key instrument deployed in this study is a HR-TOF-AMS from December 7th 2016 to January 8th 2017 Air was sampled through a PM_{10} impactor (16.7 L min^{-1}) with an automatic aerosol dryer unit to dry the sampling air with RH < 30%. Mass concentrations of organics, sulfate, nitrate,

ammonium and chloride were measured by the HR-TOF-AMS with 1-minute time resolution. Particle number size distributions were measured by Twins Differential Mobility Particle Sizer (TDMPS, TROPOS in Germany) to further correct the collection efficiency of AMS. Based on the comparison of AMS and TDMPS data, a fixed collection efficiency (CE) of 0.6 was used. Daily $PM_{2.5}$ samples were collected on quartz filters with a high volume sampler (TISCH, TE6070VFC) from 9:00 to 9:00 during 14 haze days. Hourly trace gaseous pollutants, including NO_2 (TE, 42CTL), SO_2 (TE, 43CTL), CO (TE, 48C), NH_3 (Ecotech, EC9842) and O_3 (TE, 49C) were also monitored during the campaign. The surface hourly meteorological data including temperature (T), relative humidity (RH), wind speed (WS) and direction (WD) were monitored by an automatic weather station (AWS).

2.2 Data analysis and ^{14}C-based source apportionment

2.2.1 AMS data analysis

The HR-TOF-AMS data were analyzed by Squirrel (Version 1.62G) and Pika (Version 1.22G) to determine the mass concentrations, size distributions of NR-PM_1 species, and elemental compositions of organic aerosol. In addition, the updated Improved-Ambient method (Canagaratna et al., 2015) was used to determine the elemental ratios of OA including hydrogen to carbon (H/C), oxygen to carbon (O/C), nitrogen to carbon (N/C), and organic mass to organic carbon (OM/OC) ratios. Collection efficiency (CE) was determined based on the relationship between total PM_1 and TDMPS (Zhong et al., 2020).

PMF was applied to the high resolution mass spectra to resolve distinct OA factors (Paatero and Tapper, 1994; Ulbrich et al., 2009). The procedures for the processing of data and error matrices were detailed in Ng et al. (2011). By comparing the mass spectral profiles with previous studies and correlations with time series of tracers, five OA factors with fpeak = 0 were selected, including three POA factors: HOA, CCOA and BBOA, and two SOA factors: oxidized coal combustion OA (OCCOA) and MO-OOA. The diagnostic plots and the temporal series of five OA factors with other tracers are shown in the Figures S1 and S2. The mass spectral pattern of HOA was primarily characterized by high m/z 43 and m/z 57, which are also widely used as a HOA tracer. CCOA was characterized by aromatic hydrocarbon related fragments including C_6H_5, C_7H_7 and C_9H_7, which are considered as typical tracers for coal combustion OA. OCCOA was featured by slightly higher m/z 44 signal as well as its similar mass spectral pattern with that of the CCOA, which indicated it is most likely the oxidized form of CCOA. Prominent signals at m/z 60 and 73 are used as tracers for BBOA. Significant m/z 44 signals were used to as the tracer for more oxidized OOA. Moreover, good correlations between these OA components and specific tracers confirmed the PMF results are reasonable, i.e. HOA vs C_4H_9 (fragment of alkanes), CCOA vs chloride and SO_2, OCCOA vs AH-related fragments, BBOA vs Levoglucosan, MO-OOA vs CO_2^+, sulfate and nitrate (Figure S2).

2.2.2 ^{14}C Analysis of the Carbonaceous Fractions

A punch of the daily $PM_{2.5}$ filter samples (total 14 filters) was analyzed for total carbon (TC), organic carbon (OC) and elemental carbon (EC) by the thermal optical reflectance (TOR) method following the Interagency Monitoring of Protected Visual Environments (IMPROVE) protocol (Cao et al., 2004). Another portion of the filter samples was used for ^{14}C analysis.

The OC and EC were also extracted by the IMPROVE protocol for ^{14}C measurements. Detailed descriptions of extracting procedures for OC and EC, as well as preparing procedures of

graphitization samples for OC and EC were given by Pang et al. (2019). ^{14}C measurements were performed at China Institute of Atomic Energy (CIAE) compact accelerator mass spectrometry system, which was based on a 200 kV single-stage accelerator mass spectrometer (SSAMS) (Pang et al., 2017).

^{14}C measurement results were expressed as fractions of modern C (f_M), representing the fraction of ^{14}C in the sample. In this paper, all the reported fractions of modern carbon (descript as f_{NF}) were corrected by the reference sample in year 1950. In specific, non-fossil fractions of OC and EC (i.e. f_{NF} (OC) and f_{NF} (EC), respectively) were calculated from the f_M (sample) and the reference values f_M (Ref) ($f_{NF} = f_M$ (sample)/ f_M (Ref)). More details of the estimation of reference values (f_M (Ref)) have been previously reported (Minguillón et al., 2011; Zhang et al., 2013), f_M (Ref) values were 1.07±0.04 and 1.10±0.05 for OC and EC, respectively (Zhang et al., 2017a).

2.2.3 Extended Gelencsér (EG) method for source apportionment

Based on the AMS-PMF results, mass concentrations of OC and EC and the ^{14}C results, four main parameters including EC from fossil (EC_{FF}) and non-fossil sources (EC_{NF}), OC from fossil (OC_{FF}) and non-fossil sources (OC_{NF}) were resolved. Gelencsér et al. (2007) reported a method for the source apportionment of carbonaceous aerosol into fractions from biomass burning, road traffic and secondary organic aerosol, applicable to Europe where these are the dominant sources. But in China, coal combustion fraction must be considered. The quantification of non-fossil sources of SOC by Gelencsér et al. (2007) method is dependent on the source apportionment of OC from biomass burning. But the diversity of fuel types and combustion conditions make the selection of OC/EC ratios for biomass burning aerosol difficult due to large variabilities (Hou et al., 2021). For this reason, an extended Gelencsér (EG) method (Hou et al., 2021) was used to quantify the fossil and non-fossil sources of OC (OC_{FF} and OC_{NF}) along with OC from biomass burning. Finally, OC_{FF} and OC_{NF} were further classified into subtypes including primary fossil-fuel OC (POC_{FF}), secondary fossil-fuel OC (SOC_{FF}), non-fossil OC from biomass burning OC_{bb} and other emission OC_{other}.

Hydrocarbon OC (HOC), Coal Combustion OC (CCOC), Biomass Burning OC (BBOC), Oxygenic Coal Combustion OC (OCCOC) and OC_{AMS} were calculated from HOA (Hydrocarbon OA), CCOA (Coal Combustion OA), BBOA (Biomass Burning OA), OCCOA (Oxidized CCOA) and Organics divided by corresponding OM/OC values from AMS-PMF and AMS on-line data respectively (see Figure S1). We assume that the fossil POC is the sum of HOC and CCOC, and BBOC was all from biomass burning emissions. The equations for the detailed source apportionment are shown in Table1.

Table 1. Equations for the ^{14}C based source apportionment

	Extended Gelencsér method
EC_{NF}	$EC_{bb} = f_{NF}$ (EC)×EC
EC_{FF}	$EC-EC_{NF}$
OC_{NF}	f_{NF} (OC)×OC
OC_{FF}	$OC- OC_{NF}$
POC_{FF}	$EC_{FF} \times (POC/EC)_{FF}$
SOC_{FF}	$OC_{FF}-POC_{FF}$
OC_{bb}	$EC_{NF} \times (POC/EC)_{bb}$

OC_{other}	OC_{NF}-OC_{bb}
OC_{AMS}	OA_{AMS} / $(OM/OC)_{AMS}$

where, subscripts NF, FF, and bb are abbreviation of non-fossil, fossil fuel, biomass burning respectively, and f_{NF} represents the ^{14}C fraction of non-fossil fuel sources.

To estimate the concentration of POC_{FF}, it is essential to calculate the $(POC/EC)_{FF}$. Hou et al. (2020) employed the lowest value method to calculate the $(POC/EC)_{FF}$ by $(POC/EC)_{FF,\ min}$. We followed their method to estimate $(POC/EC)_{FF,\ min}$ value by multiplying the lowest 5% OC/EC ratios with the lowest two ($\frac{1-f_{NF,OC}}{1-f_{NF,EC}}$) ratios. The estimated $(POC/EC)_{FF}$ in this study is 3.81, which is close to that reported in in Beijing (IAP site) during the winter 2016 (Hou et al., 2020). The small difference could be due to the diversity of fuel types, uncertainties of sampling and the analyzing process. Overall, the uncertainty of POC_{FF} is estimated to be 5%.

$(POC/EC)_{bb}$ is a key parameter to estimate OC_{bb}. The diversity of fuel types and combustion conditions make the selection of OC/EC ratios for biomass burning aerosol difficult. Wheat and maize straws were the two dominant biofuel in North China because they are the two most common crops (Chen et al., 2017). Biomass fuels (such as wood and straw) are widely used as the domestic fuel for cooking/heating in rural areas (Chen et al., 2017). With the help of ratios of levoglucosan to galactosan (LG/GA) and mannosan (LG/MN), Hou et al. (2021) suggested that wood in Beijing (both IAP and Pinggu sites) is likely the dominant biofuel in winter. In this study, we also determined the LG/MN and OC/LG ratios (Table 2). The average LG/MN ratio was 15.2±2.1 (from 11.2 to 19.9), and the OC/LG ratio was 85.7±87.1 (from 61.7 to 150.7). These results also suggest the dominance of wood combustion (Hou et al., 2021; Mazzoleni et al., 2007). Therefore, we adopted the average OC/EC value for wood branch 2.19 as $(POC/EC)_{bb}$ based on Sun et al. (2019). Straw burning activities were forbidden since 2013 in North China Plain but secret burning may still contribute to OC. This could contribute to some uncertainties in our estimate of $(POC/EC)_{bb}$.

The uncertainty of OC_{bb} is calculated to be 39.4% based on the following equation:

$$U\,(OC)_{bb}=\sqrt{U^2(POC/EC)_{bb}+U^2(EC)+U^2(f_{NF,}f_M,f_{ref})}$$

Here the uncertainty of the $(POC/EC)_{bb}$ is estimated to be 21% and that of EC_{NF} is calculated to be 33% by combining all the uncertainties from EC measurements (Pang et al., 2017). The combined uncertainty of f_{NF}, f_M and f_{ref} is 5%. Note that the uncertainty of OC_{bb} can also affect the estimation of OC_{other}.

3 Results and discussion

3.1 Overview of chemical composition and sources of PM_1

The temporal variations of major chemical species including organics, sulfate, nitrate, ammonium, and chloride (together defined as ΣOSNAC) in non-refractory-PM_1 (NR-PM_1), gaseous pollutants as well as meteorological conditions during Dec 7th 2016 and Jan 8th 2017 are displayed in Figure 2. The 10-min mass concentrations of ΣOSNAC varied dramatically, from 5.5 to 767.9 μg m^{-3} with an average concentration ± standard deviation of 153.0±94.6μg m^{-3}, which is about 20% higher than that in Beijing during the same period (135.8 μg m^{-3}) (Zhang et al., 2020). Daily PM_1 mass concentration exceeded the Chinese $PM_{2.5}$ standard level (75 μg m^{-3}) in 28 out of 31 days during the field campaign. The average mass concentration of organics, sulfate, nitrate, ammonium and chloride was 95.8±34.2, 22.4±11.6, 18.1±6.6, 14.4±5.1 and 9.1±3.6μg m^{-3} (Table 2). The mass

concentration of SO_2, NO_2, NH_3, and O_3 was 15.8, 46.4, 35.9, 3.4 ppb respectively, and the average CO was 3.89 ppm. SO_2 is about twice of that in Beijing (8.1ppb) during the same period. Mean relative humidity was 79% (from 30% to 100%) and the average temperature and solar radiations was -1.5 °C and 62 W m^{-2} respectively. Wind roses show that about 12% of wind is from south and 7% from southwest (Figure S3). The average wind speed is only 0.9 m s^{-1}.

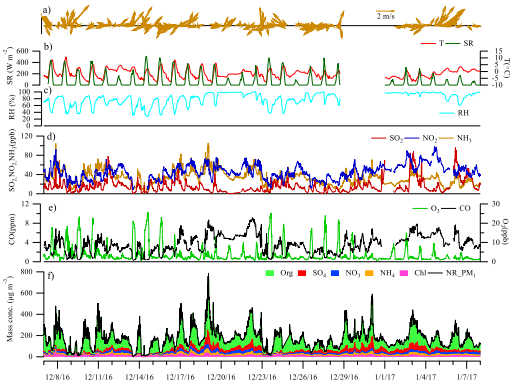

Figure 2. Time series of wind speed and direction (a), solar radiation (left) and temperature (right) (b), relative humidity (c), gaseous pollutants SO_2, NO_2, NH_3 (d) and O_3, CO(e), and PM_1 chemical species (f)

Fig. 2 shows that organics was the predominant NR-PM_1 species in Gucheng. They are about 1.5 times higher than that of the inorganic species. The mass concentrations of organics, sulfate, nitrate, ammonium and chloride was 58.9, 21.8, 30.7, 19.2 and 5.2 μg m^{-3} at an urban site in Beijing during the same period (Zhang et al., 2018). The organic aerosol in Gucheng was about 50% higher than that in Beijing. This suggests a significant local emissions and/or regional transport (Li et al., 2020). Nitrate and ammonium levels are lower than that in Beijing, and there is no obvious difference in sulfate levels at the two sites. Since 2013, coal boilers were banned in Beijing urban area, and SO_2 emission reduced dramatically (Vu et al., 2019). Much of the sulfate and SO_2 in Beijing comes from the regional transport (Zhang et al., 2018). Under the synoptic meteorological conditions, the mechanisms of sulfate formation in Beijing and Gucheng are likely to be similar. The lower concentration of nitrate in Gucheng may be ascribed to the lower road traffic emissions than that in Beijing. Higher ammonium concentration in Beijing could be due to urban emissions of non-agricultural NH_3 in the winter and complex NH_3-NH_4^+ chemistry (Wu et al., 2019).

Table 2. Statistics of the chemical species by AMS measurement and filter analysis including LG,

MN, OC, EC (unit: μg m^{-3}) and OC/EC ratio

Organics	Sulfate	Nitrate	Ammonium	Chloride	OC	EC
95.7±34.2	22.4±11.6	18.1±6.6	14.4±5.1	9.1±3.6	67.8±25.4	11.4±3.4

HOA	CCOA	BBOA	OCCOA	MO-OOA	LG	MN
11.1±5.9	36.5±21.6	9.1±6.1	11.1±4.7	28.0±13.7	0.77±0.27	0.05±0.02

Note: HOA=Hydrocarbon organic aerosol, CCOA=coal combustion organic aerosol, BBOA= biomass burning organic aerosol, OCCOA=oxidized coal combustion organic aerosol and MO-OOA =more oxygenic organic aerosol; OC_{AMS}=OA_{AMS} / $(OM/OC)_{AMS}$; LG= levoglucosan, MN= mannasan

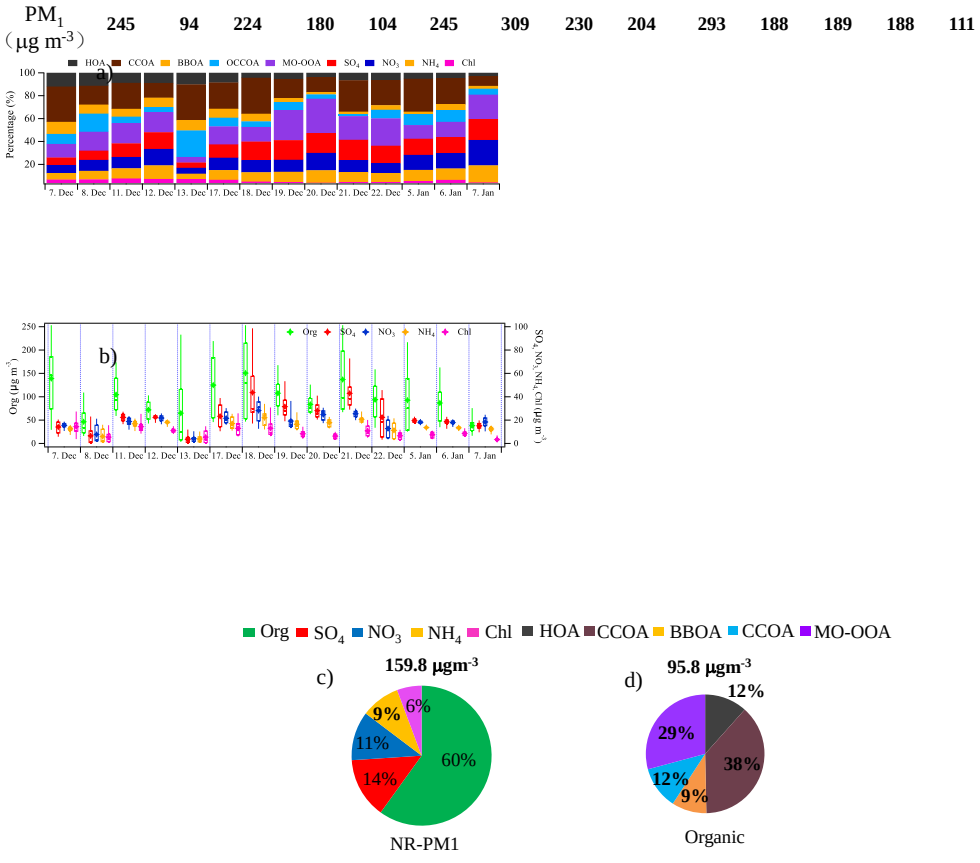

Figure 3. Temporal variations of chemical components in NR-PM_1 (a); box plot of the chemical species for organics (left axis), sulfate, nitrate, ammonium and chloride (right axis) in PM_1 with mean (line in the middle of boxes), median (cross in the middle of boxes), 5%, 25%, 75% and 95% percentiles (b); and pie charts of non-refractory species (c) and organic components (d) during the study period.

Figure 3 presents daily concentrations of chemical species as well as the AMS-PMF resolved organics in Gucheng. The average concentration of OAs from solid fuel combustion, including CCOA, OCCOA and BBOA, was 36.5±22.2, 11.1±4.8, 9.1±6.3 μg m^{-3} (Table 2), contributing 38%, 12% and 9% to total OA (Figure 3d). HOA, which is typically considered as traffic-related source accounted for 12% of total OA. In total, primary organic sources (POA) including HOA, CCOA and BBOA contributed 59% to OA. The high contribution of CCOA and OCCOA to total OA suggest a strong influence of coal combustion in Gucheng. As MO-OOA was characterized with higher O/C

ratio (0.73), it may be a mixed source of oxidized primary OA and condensed OVOCs. But it is challenging to assign its precise emissions sources based on AMS-PMF results.

Fig. 3 shows that the chemical compositions of NR-PM_1 varied day by day. The most serious pollution events were recorded on 18th and 21st December with NR-PM_1 as high as 300 μg m^{-3}. Zhong et al (2020) attributed the accumulation of PM_1 during these pollution events to day-to-day vertical meteorological variability, particularly diminishing mixing layer height exacerbated by aerosol-radiation feedback. Low solar radiations (Figure 2b) during these days may further reduce the vertical mixing of air pollutants. Furthermore, the satellite map shows that the air masses originated from the south and southwest (such as Taiyuan in Shanxi province and Shijiazhuang) (Figure S4). It is likely that meteorological variability, regional transport and increased coal combustion activities at night all contributed to the high PM levels during these events.

3.2 Fossil and non-fossil OC and EC

Figure 4 shows the filter-based mass concentration of OC and EC as well as their modern carbon fraction (f_{NF}) in $PM_{2.5}$. Average OC concentration was 67.8±25.4μg m^{-3}, varying from 33.2 to 121.8 μg m^{-3}, while the EC concentration was 11.4±3.4 μg m^{-3}. The average modern fraction f_{NF} in EC, equivalent to EC_{bb}, was 36±8.5% with a range of 26-57%, suggesting a dominant contribution of fossil-fuel combustion to EC in Gucheng. This fraction is comparable to those in hazy days at IAP (32±3%) and Pinggu (39±7%) in wintertime (Hou et al., 2021). The observed f_{NF} in EC is mostly within the range of previous studies in urban Beijing (Liu et al., 2017; Liu et al., 2020; Zhang et al., 2017a). Non-fossil fuel fraction in EC here is also comparable to those estimated by bottom-up inventories (i.e. 39%) in China, as well as to that at a background site in South China (38%) (Zhang et al., 2014a). But it is slightly lower than those found in South Asia, where local/regional biomass burning contribution to EC was more significant than fossil fuel combustions such as Hanimaadhoo, Maldives (47%) and Sinhagad, India (49%) (Zhang et al., 2017a). In Europe, urban sites were less influenced by non-fossil EC emissions than at rural sites. For example, 13% of EC at an urban background site in Barcelona in winter was originated from non-fossil fuel combustion but this value increased to 34% at a forest regional background site - Montseny (Minguillón et al., 2011). In Goteborg, Sweden, winter non-fossil fraction f_{NF} (EC) was 12% and 39% at the urban and rural site respectively (Szidat, 2009).

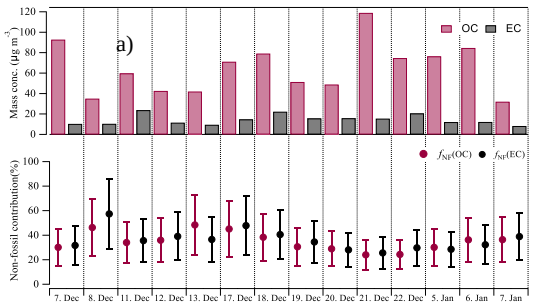

b)

Figure 4. Temporal variations of TC, OC and EC concentrations (a); and f_{NF} of OC and EC (b)

Non-fossil contribution to OC varied from 24% to 48% with a mean of 34.9±7.7%, indicating the dominant contribution of fossil-fuel combustion to OC in Gucheng. This value was comparable to that in urban Beijing (32%) in winter 2016 (Hou et al., 2021), but much lower than some European urban site (68±4%), rural site (71±4%) (Szidat et al., 2009), and forest sites (69±4%) in Goteborg, and urban background site (60±4%) at Barcelona (Minguillón et al., 2011). The more widespread use of wood for residential heating in Europe is the likely reason the for higher non-fossil fraction of OC reported there. Since 2013, open burning activities had been banned in NCP. Therefore, the main non-fossil fuel sources in Gucheng are associated with cooking and residential heating.

3.3 Source apportionment of organic carbon in Gucheng

The relative contributions of fossil and non-fossil fuel carbonaceous aerosols to TC were summarized in Figure 5. We first categorized OC and EC into fossil and non-fossil subtypes (Figure 5a). Fossil derived OC was the largest contributor to TC (53±9.4%). OC_{NF} accounted for 27% of TC. The fossil and non-fossil fuel EC contributes 13% and 7% to TC respectively.

We further classified OC into primary fossil OC (POC_{FF}), secondary fossil OC (SOC_{FF}), biomass burning OC (OC_{bb}) and other non-fossil OC (OC_{other}) using the Extended Gelenscér method (Figure 5b and Table 3). The mass concentrations of POC_{FF} and SOC_{FF} was 27.9±8.8 and 16.9±17.4 μg m^{-3}, accounting for 35% and 22% of TC, respectively. In total, about 57% of TC is attributed to fossil fuel sources. More fossil fuel OC was from the primary OC than that from the secondary OC_{FF}, indicating more local fossil fuel emissions.

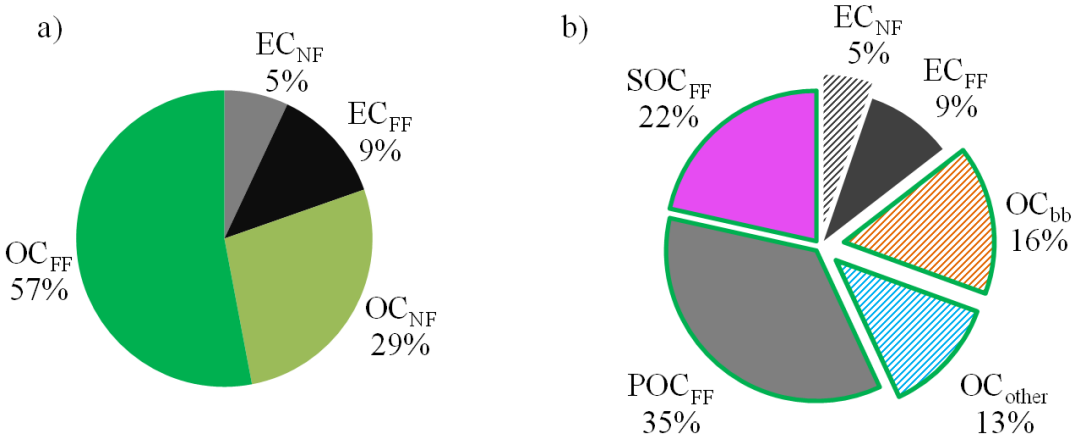

Figure 5. Relative contributions of fossil and non-fossil fuel OC and EC to TC (a); Relative contributions of EC_{NF}, EC_{FF}, POC_{FF}, SOC_{FF}, OC_{bb} and OC_{other} to TC (b)

Carbonaceous aerosol from biomass burning (EC_{NF}+OC_{bb}) is estimated to account for 21% of TC. OC_{bb} contributes 57% to OC_{NF} and 16% to the TC. Its contribution to TC is higher than that (10.4%) in Beijing in winter 2016 (Hou et al., 2021). This is reasonable because biomass fuel was widely burned for cooking and heating in rural area in Northern China (Meng et al., 2019).

OC_{other} is determined by subtracting OC_{bb} from OC_{NF}. About 13% of the TC was estimated to be OC_{other} in this study. OC_{other} represents OC from non-fossil sources excluding OC_{bb}, so it could include secondary OC from biogenic emission and primary non-biomass burning emissions, such as cooking and vegetative detritus as well as particles derived from vehicle tyre wear (e.g., from natural rubber) (Heal, 2014). A higher signal of m/z 55 than m/z 57 was widely identified as cooking OA (COA) tracers. This has been shown to work well in urban Beijing, and was confirmed with concentration peaks at noon and evening meal time (Zhang et al., 2018). But in this study, due to the absence of a high signal of m/z 55 than m/z57 and the noon and evening concentration peaks, no COA was resolved by the AMS-PMF method. This could be due to a relatively low contribution of cooking to OA at Gucheng as a result of relatively low population density than in cities.

Our results support the emission inventory-based study by Meng et al. (2019) who suggested a significant contribution of solid fuel consumption, particularly coal, on ambient $PM_{2.5}$ levels in NCP. Zhang et al. (2021) and Liu et al. (2021) also found strong evidence of the organic aerosols emitted from the residential sector by using single particle analyses, although they did not provide a quantitative source apportionment.

Table 3. Statistics of resolved categories of OC as well as fossil and non-fossil sources of POC and SOC (unit: μg m^{-3})

f_{NF}(OC)(%)	f_{NF}(EC)(%)	OC_{NF}	OC_{FF}	EC_{NF}
34.9±7.7	36.1±8.5	22.5±6.9	45.3±20.6	4.1±1.6
EC_{FF}	OC_{bb}	OC_{other}	POC_{FF}	SOC_{FF}
7.3±2.3	12.6±4.2	9.9±6.4	27.9±8.8	16.9±17.4

Correlations of resolved OC categories based on the EG method and AMS-PMF method are

further investigated. POC_{FF} displays a good correlation with CCOC, CCOC+HOC and sulfate, with R^2 of 0.55, 0.57 and 0.61 respectively (Figure 6a, b, c), while the slope between CCOC and POC_{FF} was close to 1 (0.96) and that between CCOC+HOC and POC_{FF} was 1.22. These results suggest an overestimation of primary fossil emission from the AMS. This could be due to the uncertainties in AMS-PMF analysis. For example, cooking OA may be misinterpreted as HOC (Sun et al., 2018), leading to an overestimation of the HOC.

Good correlations were also found between BBOC by AMS-PMF and calculated OC_{bb} and POC_{NF} by the EG method (R^2 =0.58 and 0.65) (Figure 6). The slope shows that AMS-PMF based BBOC was less than half of the OC_{bb}. One of the possible reasons is that some primary biomass burning OC having been oxidized into OOA during the haze events, and mixed with other types of OOA. With the aid of OM/OC ratio (1.75) from AMS (Figure S2) and the calculated OC_{bb}, organics from biomass burning emission are estimated to be 22.1 μg m^{-3}, accounting for 23% of total OA. If excluding the BBOA estimated from AMS-PMF, oxygenated BBOA (OBBOA) was estimated to be 12.8 μg m^{-3}, contributing to 44.5% of MO-OOA. Using levoglucan as a tracer of biomass burning aerosol, we found that OC_{bb}/LG ratio was 13.4 and their correlation coefficient R^2 was 0.49, which is comparable to the widely used value (12.2) in previous studies (Zhang et al., 2008; Zhang et al., 2007).

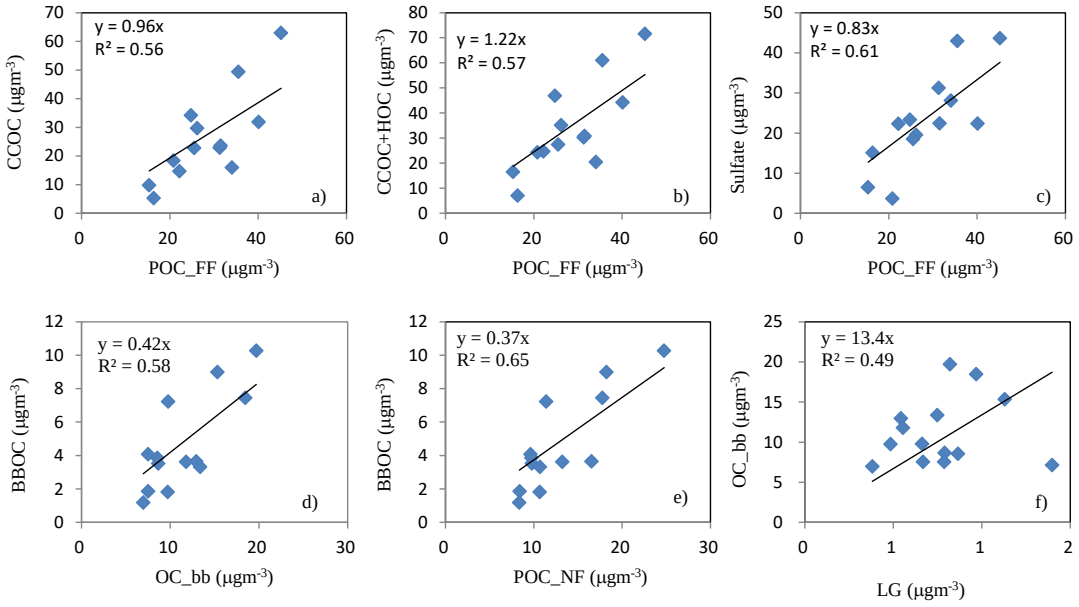

Figure 6. Correlations between the resolved OC categories based on the EG method and AMS-PMF method

4. Conclusions

Our study showed that the mass concentrations of the total non-refractory PM_1 (ΣOSNAC) from 7th Dec 2016 to 8th Jan 2017 at the rural site of Gucheng was about 20% higher than that in Beijing (153.0±94.6 vs. 135.8 μg m^{-3}). This suggests that the rural areas in NCP may be a significant source of air pollution to surrounding megacities such as Beijing and Tianjin in winter. Organic aerosol was the predominant species in Gucheng, accounting for 60% of total NR-PM_1. Fossil fuel combustion, predominantly coal burning, accounted for 66% of TC in $PM_{2.5}$. Biomass burning

contributed to about 21% of TC. These results indicated that solid fuel combustion was the major source of air pollution in winter 2016 in the rural area. This confirms the need (and benefit) of the transition to cleaner energy for the residential sector, not only for improving air quality for the rural but also the urban residents.

Supplementary file

The supplement file include mass spectrums of the different types of OAs during studied period (Figure S1); Time series of resolved organic components, other independent species including C_4H_9, Chloride, SO_2 (g), Aromatic Hydrogen (AH)-related (including C_6H_5+C_7H_7+C_9H_7), $C_2H_4O_2$, sulfate (Figure S2); Wind rose during studied period in Gucheng site (Figure S3); The satellite pictures by MODIS combined values from Terra and Aqua data during 16-21 December in 2016 (Figure S4).

Author Information

Correspondence to: YM Zhang (ymzhang@cams.ac.uk) and ZB Shi (z.shi@bham.ac.uk)

Funding Information

This study was supported by the National Natural Science Foundation of China (41675121 and 41775121) and Chinese Government Scholarship (CSC NO. 202105330037). Z.S. is funded by UK Natural Environment Research Council (Grant no. NE/R005281/1 and NE/N007190/1). The study was also supported by the Innovation Team for Haze-fog Observation and Forecasts of MOST.

References

GBD MAPS Working Group:Burden of Disease Attributable to Coal-Burning and Other Major Sources of Air Pollution in China,Special Report 20. Health Effects Institute. Boston, MA, 2016.

Canagaratna, M. R., et al., 2015. Elemental ratio measurements of organic compounds using aerosol mass spectrometry: characterization, improved calibration, and implications. Atmos. Chem. Phys. 15**,** 253–272**.** https://doi.org/10.5194/acp-15-253-2015.

Canonaco, F., et al., 2013. SoFi, an Igor based interface for the efficient use of the generalized multilinear engine (ME-2) for source apportionment: application to aerosol mass spectrometer data. Atmos. Meas. Tech. 6**,** 3649–3661**.** https://doi.org/10.5194/amt-6-3649-2013.

Cao, J. J., et al., 2004. Spatial and seasonal variations of atmospheric organic carbon and elemental carbon in Pearl River Delta Region, China. Atmos.Environ. 38**,** 4447-4456**.** https://doi.org/10.1016/j.atmosenv.2004.05.016.

Chen, J., et al., 2017. A review of biomass burning: emissions and impacts on air quality, health and climate in China. Sci.Total Environ. 579**,** 1000-1034**.** http://dx.doi.org/10.1016/j.scitotenv.2016.11.025.

Cheng, J., et al., 2018. Dominant role of emission reduction in PM2.5 air quality improvement in Beijing during 2013-2017: a model-based decomposition analysis. Atmos. Chem. Phys. 6125–6146**.** https://doi.org/10.5194/acp-19-6125-2019.

Cheng, J., et al., 2021. Pathways of China's PM2.5 air quality 2015–2060 in the context of carbon neutrality. Natl. Sci. Rev. nwab078**,** 1-11**.** https://doi.org/10.1093/nsr/nwab078.

Costa, M., et al., 2015. Split Injection in a GDI Engine Under Knock Conditions: An Experimental and Numerical Investigation. SAE Technical Paper. 24-2432**.**

Fan, Y., et al., 2020. Large contributions of biogenic and anthropogenic sources to fine organic aerosols

in Tianjin, North China. Atmos. Chem. Phys. 20, 117-137. https://doi.org/10.5194/acp-20-117-2020.
He, Y., et al., 2021. Changes of ammonia concentrations in wintertime on the North China Plain from 2018 to 2020. Atmos. Res. 253, 105490. https://doi.org/10.1016/j.atmosres.2021.105490.
Heal, M. R., 2014. The application of carbon-14 analyses to the source apportionment of atmospheric carbonaceous particulate matter: a review. Anal. Bioanal. Chem. 406, 81-98. https://doi.org/10.1007/s00216-013-7404-1.
Hopke, P. K., et al., 2020. Global review of recent source apportionments for airborne particulate matter. Sci.Total Environ. 740. https://doi.org/10.1016/j.scitotenv.2020.140091.
Hou, S., et al., 2021. Source Apportionment of Carbonaceous Aerosols in Beijing with Radiocarbon and Organic Tracers: Insight into the Differences between Urban and Rural Sites. Atmos. Chem. Phys. 21, 8273-8292. https://doi.org/10.5194/acp-21-8273-2021.
IPCC, 2021. Sixth assessment report: Climate change 2021 The physical science basis.
Jimenez, J. L., et al., 2009. Evolution of Organic Aerosols in the Atmosphere. Science. 326, 1525-1529. https://doi.org/10.1126/science.1180353.
Kuang, Y., et al., 2020. Photochemical Aqueous-Phase Reactions Induce Rapid Daytime Formation of Oxygenated Organic Aerosol on the North China Plain. Environ. Sci. Technol. 54, 3849-3860. https://dx.doi.org/10.1021/acs.est.9b06836.
Li, G., et al., 2021a. Multiphase chemistry experiment in Fogs and Aerosols in the North China Plain (McFAN): integrated analysis and intensive winter campaign 2018. Faraday Discus.~~sions.~~ 226, 1-16. http://doi.org/10.1039/d0fd00099j.
~~Li, G., et al., 2020. Multiphase chemistry experiment in Fogs and Aerosols in the North China Plain (McFAN): integrated analysis and intensive winter campaign 2018. Faraday Discussions. 10.1039/d0fd00099j.~~
Li, J., et al., 2017a. Rapid formation of a severe regional winter haze episode over a mega- city cluster on the North China Plain. Environ. Pol. 223, 605-615. http://dx.doi.org/10.1016/j.envpol.2017.01.063.
Li, J., et al., 2021b. Significant changes in autumn and winter aerosol composition and sources in Beijing from 2012 to 2018: Effects of clean air actions. Environ. Pol. 268, 1-10. https://doi.org/10.1016/j.envpol.2020.115855.
Li, Y. J., et al., 2017b. Real-time chemical characterization of atmospheric particulate matter in China: A review. Atmos. Environ. 158, 270-304. http://dx.doi.org/10.1016/j.atmosenv.2017.02.027.
Liang, C. S., et al., 2016. Review on recent progress in observations, source identifications and countermeasures of $PM_{2.5}$. Environ. Int. 86, 150-170. http://dx.doi.org/10.1016/j.envint.2015.10.016.
Lin, W., et al., 2009. Characteristics of gaseous pollutants at Gucheng, a rural site southwest of Beijing. J. Geophys. Res.: Atmos. 114, D00G14,. https://doi.org/10.1029/2008JD010339.
Liu, D., et al., 2017. Sources of non-fossil-fuel emissions in carbonaceous aerosols during early winter in Chinese cities. Atmos. Chem.Phys. 17, 11491-11502. https://doi.org/10.5194/acp-2017-340.
Liu, D., et al., 2020. Fossil and non-fossil fuel sources of organic and elemental carbon aerosols in Beijing, Shanghai and Guangzhou: Seasonal carbon-source variation. Aerosol. Air. Qual. Res. 20, 2495–2506. https://doi.org/10.4209/aaqr.2019.12.0642.
Liu, X. Y., et al., 2019. Analysis of the origins of black carbon and carbon monoxide transported to Beijing, Tianjin, and Hebei in China. Sci. Total Environ. 653, 1364-1376. https://doi.org/10.1016/j.scitotenv.2018.09.274.

Marseglia, G., et al., 2019. Experimental and numericaltechniques to detect pollutant formation in transport sector. WIT Press.

Mazzoleni, L. R., et al., 2007. Emissions of levoglucosan, methoxy phenols, and organic acids from prescribed burns, laboratory combustion of wildland fuels, and residential wood combustion. Environ. Sci. Technol. 41(7), 2115-2122. http://doi.org/10.1021/es061702c.

Meng, W., et al., 2019. Energy and air pollution benefits of household fuel policies in northern China. PNAS. 116, 16773–16780. www.pnas.org/cgi/doi/10.1073/pnas.1904182116.

Minguillón, M. C., et al., 2011. Fossil versus contemporary sources of fine elemental and organic carbonaceous particulate matter during the DAURE campaign in Northeast Spain. Atmos. Chem. Phys. 11, 12067-12084. https://doi.org/10.5194/acp-11-12067-2011.

Paatero, P., Tapper, U., 1994. Positive matrix factorization: A non-negative factor model with optimal utilization of error estimates of data values. Environmetrics. 5, 111-126.

Panagi, M., et al., 2020. Investigating the regional contributions to air pollution in Beijing: a dispersion modelling study using CO as a tracer. Atmos. Chem. Phys. 20, 2825-2838. https://doi.org/10.5194/acp-20-2825-2020.

Pang, Y., et al., 2017. Study of 14C sample preparation for low energy single stage AMS. Atomic Energy Science and Technology. 51, 1866-1873. http://doi.org/10.7538/yzk.2017.youxian.0012.

Pope, C. A., III, Dockery, D. W., 2006. Health effects of fine particulate air pollution: Lines that connect. J. Air Waste Manage. Assoc. 56, 709-742. https://doi.org/10.1080/10473289.2006.10464485.

Pope III, C. A., et al., 2002. Lung cancer, cardiopulmonary mortality, and long-term exposure to fine particulate air pollution. J. Am. Med. Assoc. 287, 1132-1141. https://doi.org/10.1001/jama.287.9.1132

Shi, Z., et al., 2021. Atmospheric pollution and human health in a Chinese megacity (APHHBeijing) programme: final report. https://dio.org/10.25500/epapers.bham.00003381.

Sillanpää, M., et al., 2005. Organic, elemental and inorganic carbon in particulate matter of six urban environments in Europe. Atmos. Chem. Phys. 5, 2869-2879. https://doi.org/10.5194/acp-5-2869-2005.

Su, F., et al., 2004. Convergence System of Air Contamination in Boundary Layer above Beijing and North China: Transportation Convergence in Boundary Layer (in Chinese). Research of Enviornmental Sciences. 17(1), 21-33.

Sun, J., et al., 2019. Characterization of PM2.5 source profiles from typical biomass burning of maize straw, wheat straw, wood branch, and their processed products (briquette and charcoal) in China. Atmos. Environ. 205, 36-45. https://doi.org/10.1016/j.atmosenv.2019.02.038.

Sun, Y., et al., 2015. Rapid formation and evolution of an extreme haze episode in Northern China during winter 2015. Scientific Reports. 6:27151, 1-9. http://doi.org/10.1038/srep27151.

Sun, Y., et al., 2018. Source apportionment of organic aerosol from 2-year highly time-resolved measurements by an aerosol chemical speciation monitor in Beijing, China. Atmos. Chem. Phys. 18, 8469-8489. https://doi.org/10.5194/acp-18-8469-2018.

Szidat, S., 2009. Sources of Asian haze. Science. 323, 470-471. https://doi.org/10.1126/science.1169407.

Szidat, S., et al., 2009. Fossil and non-fossil sources of organic carbon (OC) and elemental carbon (EC) in Goteborg, Sweden. Atmos. Chem. Phys. 9, 1521-1535. www.atmos-chem-phys.net/9/1521/2009/.

Takegawa, N., et al., 2009. Variability of submicron aerosol observed at a rural site in Beijing in the summer of 2006. J. Geophys. Res.: Atmos.. 114, D00G05. https://doi.org/10.1029/2008JD010857.

Ulbrich, I. M., et al., 2009. Interpretation of organic components from Positive Matrix Factorization of

aerosol mass spectrometric data. Atmos. Chem. Phys. 9, 2891-2918. www.atmos-chem-phys.net/9/2891/2009/.

Vu, T. V., et al., 2019. Assessing the impact of Clean Air Action Plan on Air Quality Trends in Beijing Megacity using a machine learning technique. Atmos. Chem. Phys. 19, 11303–11314. https://doi.org/10.5194/acp-19-11303-2019.

Wang, F., et al., 2021a. Review of online source apportionment research based on observation for ambient particulate matter. Sci. Total Environ. 762, 144095. https://doi.org/10.1016/j.scitotenv.2020.144095.

Wang, J., et al., 2021b. Aqueous production of secondary organic aerosol from fossil-fuel emissions in winter Beijing haze. PNAS. 118, 1-6. https://doi.org/10.1073/pnas.2022179118.

Wang, M., et al., 2021c. Chemical characteristics and sources of nitrogen-containing organic compounds at a regional site in the North China Plain during the transition period of autumn and winter. Sci. Total Environ. 13, 151451. https://doi.org/10.1016/j.scitotenv.2021.151451.

Wang, Y., et al., 2020. Chemical composition and sources of submicron aerosols in winter at a regional site in Beijing-Tianjin-Hebei region: Implications for the Joint Action Plan. Sci. Total Environ. 719, 137547. https://doi.org/10.1016/j.scitotenv.2020.137547.

Watson, J. G., 2002. Visibility: Science and regulation. J. Air Waste Manage. Assoc. 52, 628-713. https://doi.org/10.1080/10473289.2002.10470813.

WHO, 2021. WHO global air quality guidelines. Particulate matter (PM2.5 and PM10), ozone, nitrogen dioxide, sulfur dioxide and carbon monoxide. ISBN 978-92-4-003422-8.

Wu, L., et al., 2019. Aerosol Ammonium in the Urban Boundary Layer in Beijing: Insights from Nitrogen Isotope Ratios and Simulations in Summer 2015. Environ. Sci. Technol. Lett. 6, 389-395. http://doi.org/10.1021/acs.estlett.9b00328.

Xia, Y., et al., 2016. Assessment of socioeconomic costs to China's air pollution. Atmos. Environ. 139, 147-156. http://dx.doi.org/10.1016/j.atmosenv.2016.05.036.

Xu, J., et al., 2020. An evaluation of source apportionment of fine OC and PM2.5 by multiple methods: APHH-Beijing campaigns as a case study. Faraday Discuss. https://doi.org/10.1039/D0FD00095G.

Xu, W., et al., 2021. Size-resolved characterization of organic aerosol in the North China Plain: new insights from high resolution spectral analysis. Environ. Sci.: Atmos. 1, 346-358. https://doi.org/10.1039/d1ea00025j.

Zhang, T., et al., 2008. Identification and estimation of the biomass burning contribution to Beijing aerosol using levoglucosan as a molecular marker. Atmos. Environ. 42, 7013-7021. https://doi.org/10.1016/j.atmosenv.2008.04.050.

Zhang, Y., et al., 2017a. High Contribution of Nonfossil Sources to Submicrometer Organic Aerosols in Beijing, China. Environ. Sci. Technol. . 51, 7842-7852. https://doi.org/10.1021/acs.est.7b01517.

Zhang, Y., et al., 2007. Source profiles of particulate organic matters emitted from cereal straw burnings. J. Environ. Sci. 19, 167-175. http://doi.org/10.1016/s1001-0742(07)60027-8.

Zhang, Y., et al., 2020. Significant changes in chemistry of fine particles in wintertime Beijing from 2007 to 2017: Impact of clean air actions. Environ. Sci. Technol. 54, 1344-1352. https://doi.org/10.1021/acs.est.9b04678.

Zhang, Y., et al., 2018. Chemical components, variation, and source identification of PM1 during Heavy Air Pollution Episodes in Beijing. J. Meteor. Res. 32, 1-13. https://doi.org/10.1007/s13351-018-7051-8.

Zhang, Y. L., et al., 2014a. Radiocarbon-Based Source Apportionment of Carbonaceous Aerosols at a Regional Background Site on Hainan Island, South China. Environ. Sci. Technol. 48, 2651-2659.

https://dx.doi.org/10.1021/es4050852.
Zhang, Y. L., et al., 2013. Fossil and non-fossil sources of different carbonaceous fractions in fine and coarse particles by radiocarbon measurement. Radiocarbon 55, 1510-1520. https://doi.org/10.1017/S0033822200048438
Zhang, Y. M., Characterization of sub-micron aerosol and its change processes in BIV (Beijing and its vicinity) region. Vol. PhD. Chinese Academy of Meteorological Sciences, Beijing, 2011.
Zhang, Y. M., et al., 2014b. Chemical composition and mass size distribution of PM 1 at an elevated site in central east China. Atmos. Chem. Phys. 14, 12237-12249. https://doi.org/10.5194/acp-14-12237-2014.
Zhang, Z., et al., 2017b. Characteristics of chemical composition and role of meteorological factors during heavy aerosol pollution episodes in northern Beijing area in autumn and winter of 2015. Tellus B. 69:1, 1347484. http://dx.doi.org/10.1080/16000889.2017.1347484.
Zheng, G. J., et al., 2015. Exploring the severe winter haze in Beijing: the impact of synoptic weather, regional transport and heterogeneous reactions. Atmos. Chem. Phys. 15, 2969-2983. https://doi.org/10.5194/acp-15-2969-2015.
Zhong, J., et al., 2020. Drivers of the rapid rise and daily-based accumulation in PM1. Sci.Total Environ. 760, 143394. https://doi.org/10.1016/j.scitotenv.2020.143394.
Zhou, W., et al., 2020. A review of aerosol chemistry in Asia: insights from aerosol mass spectrometer measurements. Environ. Sci.: Proc. Impacts 22, 1616-1653. https://doi.org/10.1039/d0em00212g.
Zhou, Y., et al., 2017. A comprehensive biomass burning emission inventory with high spatial and temporal resolution in China. Atmos. Chem. Phys. 17, 2839-2864. http://doi.org/10.5194/acp-17-2839-2017.
Zou, J., et al., 2017. Aerosol chemical compositions in the North China Plain and the impact on the visibility in Beijing and Tianjin. Atmos. Res. 201, 235-246. https://doi.org/10.1016/j.atmosres.2017.09.014.

TABLE LEGENDS:

Table 1 Equations for the ^{14}C based Source Apportionment

Table 2 Statistics of the chemical species by AMS measurement and filter analysis including LG, MN, OC, EC (unit: μg m^{-3}) and OC/EC ratio

Table 3 Statistics of resolved categories of OC as well as fossil and non-fossil sources of POC and SOC (unit: μg m^{-3})

FIGURE LEGENDS:

Figure 1 The topographic map of the NCP and the location of study site (red circle)

Figure 2. Time series of wind speed and direction (a), solar radiation (left) and temperature (right) (b), relative humidity (c), gaseous pollutants SO_2, NO_2, NH_3 (d) and O_3, CO(e), and PM_1 chemical species (f)

Figure 3. Temporal variations of chemical components in NR-PM_1 (a); box plot of the chemical species for organics (left axis), sulfate, nitrate, ammonium and chloride (right axis) in PM_1 with mean (line in the middle of boxes), median (cross in the middle of boxes), 5%, 25%, 75% and 95% percentiles (b); pie charts of non-refractory species (c) and organic components (d) during the study period.

Figure 4. Temporal variations of TC, OC and EC concentrations (a); and f_{NF} of OC and EC (b).

Figure 5. Relative contributions of fossil fuel and non-fossil OC and EC to TC (a); Relative contributions of EC_{NF}, EC_{FF}, POC_{FF}, SOC_{FF}, OC_{bb} and OC_{other} to TC (b)

Figure 6 Correlations between the resolved OC categories based on the EG method and AMS-PMF method

Table 1. Equations for the ^{14}C based Source Apportionment

	Extended Gelencsér method
EC_{NF}	$EC_{bb} = f_{NF}(EC) \times EC$
EC_{FF}	$EC\text{-}EC_{NF}$
OC_{NF}	$f_{NF}(OC) \times OC$
OC_{FF}	$OC\text{-}OC_{NF}$
POC_{FF}	$EC_{FF} \times (POC/EC)_{FF}$
SOC_{FF}	$OC_{FF}\text{-}POC_{FF}$
OC_{bb}	$EC_{NF} \times (POC/EC)_{bb}$
OC_{other}	$OC_{NF}\text{-}OC_{bb}$
OC_{AMS}	$OA_{AMS} / (OM/OC)_{AMS}$

Table 2. Statistics of the chemical species by AMS measurement and filter analysis including LG, MN, OC, EC (unit: μg m^{-3}) and OC/EC ratio

Organics	Sulfate	Nitrate	Ammonium	Chloride	OC	EC
95.7±34.2	22.4±11.6	18.1±6.6	14.4±5.1	9.1±3.6	67.8±25.4	11.4±3.4
HOA	CCOA	BBOA	OCCOA	MO-OOA	LG	MN
11.1±5.9	36.5±21.6	9.1±6.1	11.1±4.7	28.0±13.7	0.77±0.27	0.05±0.02

Note: HOA=Hydrocarbon organic aerosol, CCOA=coal combustion organic aerosol, BBOA= biomass burning organic aerosol, OCCOA=oxidized coal combustion organic aerosol and MO-OOA =more oxygenic organic aerosol; $OC_{AMS}=OA_{AMS} / (OM/OC)_{AMS}$; LG= levoglucosan, MN= mannasan

Table 3. Statistics of resolved categories of OC as well as fossil and non-fossil sources of POC and SOC (unit: μg m^{-3})

$f_{NF}(OC)(\%)$	$f_{NF}(EC)(\%)$	OC_{NF}	OC_{FF}	EC_{NF}
34.9±7.7	36.1±8.5	22.5±6.9	45.3±20.6	4.1±1.6
EC_{FF}	OC_{bb}	OC_{other}	POC_{FF}	SOC_{FF}
7.3±2.3	12.6±4.2	9.9±6.4	27.9±8.8	16.9±17.4

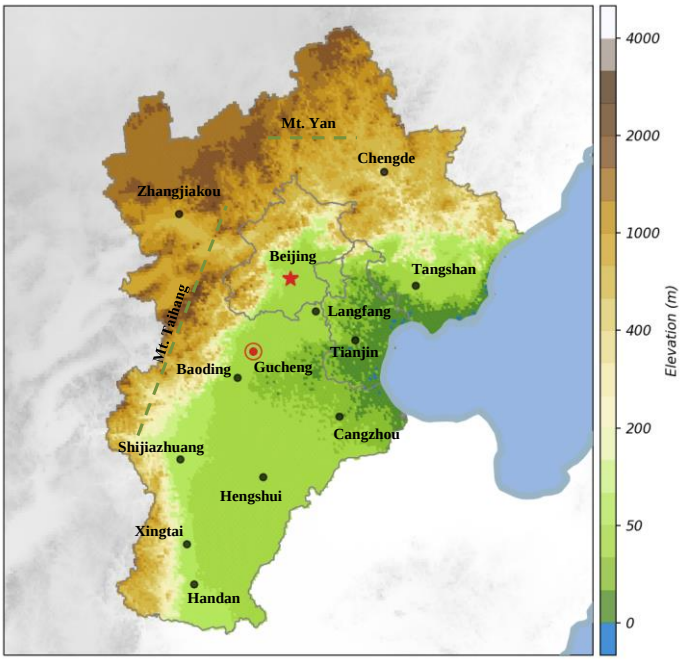

Figure1. The location of study site (red circle) and surrounding major cities in the NCP. The color scheme represents the elevation.

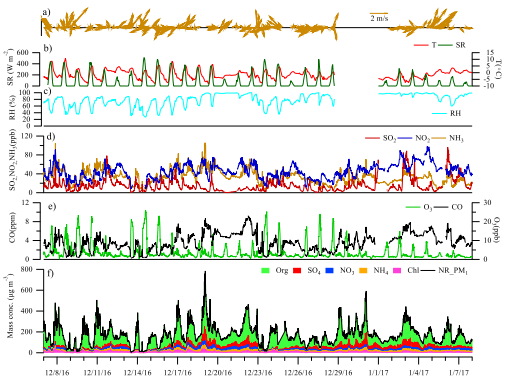

Figure 2. Time series of wind speed and direction (a), solar radiation (left) and temperature (right) (b), relative humidity (c), gaseous pollutants SO_2, NO_2, NH_3 (d) and O_3, CO(e), and PM_1 chemical species (f)

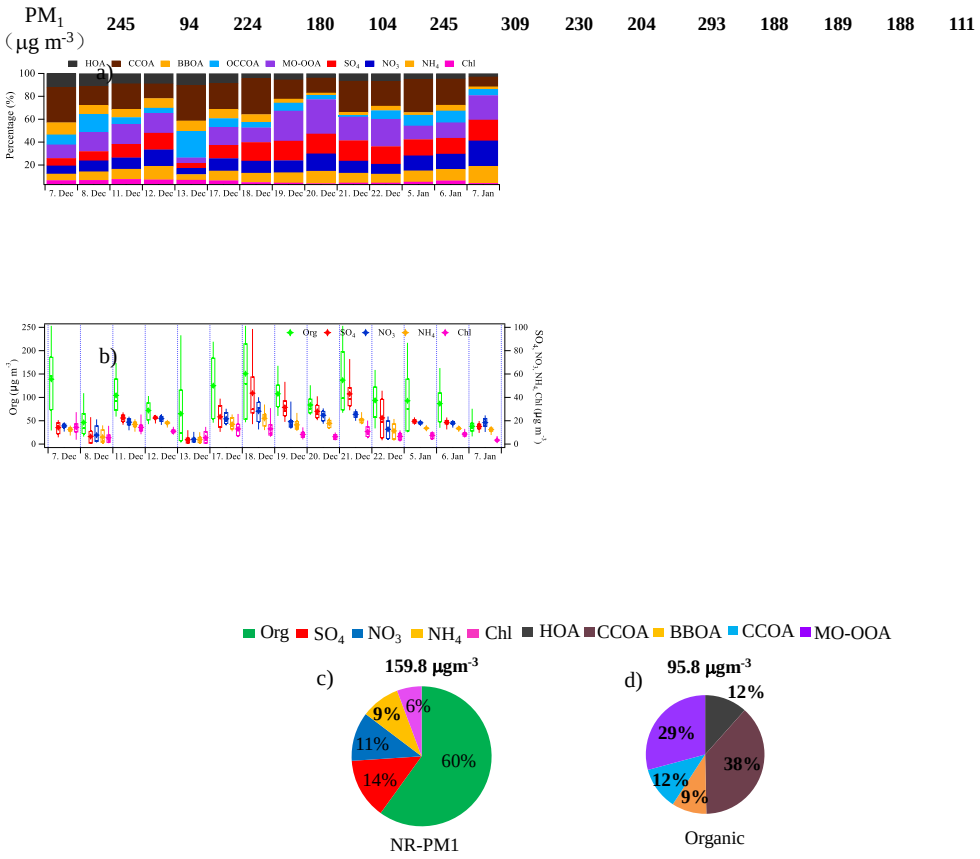

Figure 3. Temporal variations of chemical components in NR-PM_1 (a); box plot of the chemical species for organics (left axis), sulfate, nitrate, ammonium and chloride (right axis) in PM_1 with mean (line in the middle of boxes), median (cross in the middle of boxes), 5%, 25%, 75% and 95% percentiles (b); pie charts of non-refractory species (c) and organic components (d) during the study period.

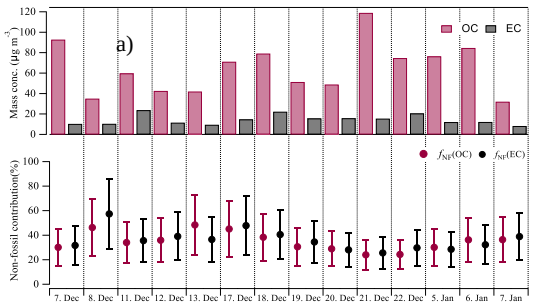

b)

Figure 4. Temporal variations of TC, OC and EC concentrations (a); and f_{NF} of OC and EC (b)

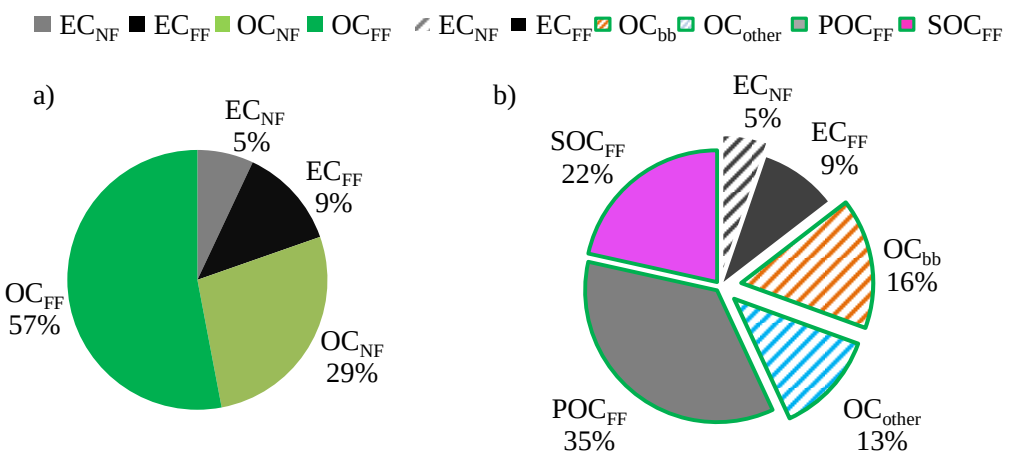

Figure 5. Relative contributions of fossil fuel and non-fossil OC and EC to TC (a); Relative contributions of EC_{NF}, EC_{FF}, POC_{FF}, SOC_{FF}, OC_{bb} and OC_{other} to TC (b)

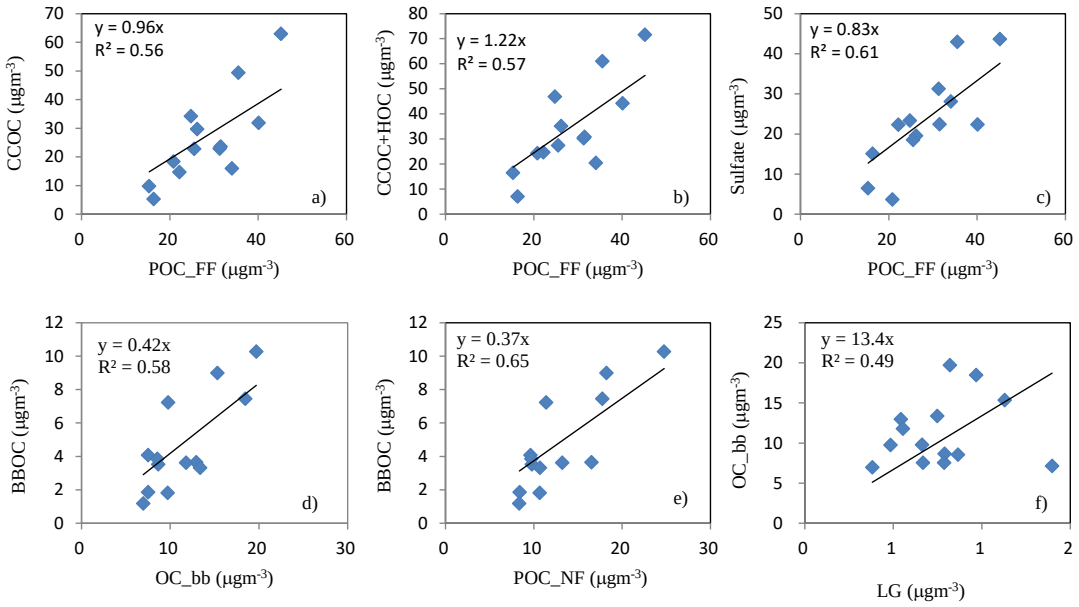

Figure 6. Correlations between the resolved OC categories based on the EG method and AMS-PMF method